*Romanian Reports in Physics, Vol. 62, No. 4, P. 758–770, 2010*



# PULSED LASER ABLATION OF SOLIDS

M. STAFE, C. NEGUTU, N. N. PUSCAS, I. M. POPESCU

*University "Politehnica" of Bucharest, Physics Department, 313 Splaiul Independentei, 060042 Bucharest, Romania, stafe@physics.pub.ro, negutu@physics.pub.ro*

(Received February 15, 2010)

*Abstract*. Here we give an overview on our main experimental and theoretical work on pulsed laser ablation (PLA) on several targets: metals (Al, Ti, Fe and Cu) and dielectrics ($Er^{3+}$:Ti:$LiNbO_3$). PLA is demonstrated to be effective when the laser fluence is larger than a threshold value which depends mainly on the optical properties of the material and wavelength. The experiments indicate that the ablation rate decreases approximately linearly with wavelength and with the inverse of beam diameter, whereas an increasing fluence leads to logarithmic increase of the ablation rate. Opto-dynamics and laser spectroscopy are used for analyzing the ablation plasmas and the ablated structures in real-time.

We further characterize theoretically the laser ablation and present the photo-thermal model for ablation with short pulses. We show that PLA in ns/ps regimes can be considered as a superposition of heating, melting, vaporization and melt ejection under the action of the plasma recoil pressure, the plasma shielding effect being also accounted for. The ablation rate is calculated numerically by solving through finite-differences method a heat-type equation in an iterative algorithm and indicates, like the experiments do, that the ablation rate is first constant during the first pulses and decreases strongly afterward with increasing pulse number.

*Key words:* pulsed laser ablation, opto-acoustic method, shock wave, ablation plasmas, spectroscopic method, photo-thermal model.

## 1. CHARACTERISTICS OF PULSED LASER ABLATION (PLA)

Pulsed laser ablation (PLA) represents the process of material removing under the action of short laser pulses. PLA becomes effective when the laser fluence is larger than a threshold value $F_{th}$ which gives ablation of at least a mono-atomic layer, the threshold fluence depending on the material optical properties and, consequently, on laser wavelength [1-5]. The typical effect of PLA consists in drilling micro and nano craters and grooves at the irradiated surface. These simple structures represent the basis of micro and nano-pattern produced by

PLA which intend to modify the surface properties (i.e. hardness, hydrophobic properties, optical absorptivity) or to produce micro-components for mechanical or optical devices (microlenses for optoelectronic circuits, cooling holes for aircrafts engines [1, 2, 6, 7]).

Figs. 1 a)-d) present such 'simple' craters ablated in aluminium with 532 nm, 5 ns Nd-YAG laser pulses at different fluences obtained by using the experimental setup outlined in Fig. 1 e). These pictures demonstrate that the quality (roughness) and dimensions of the ablated craters strongly depend on the irradiation conditions such as fluence (Fig. 1a-c) and beam diameter (Fig. 1 c), d).

The advantage of PLA in micro processing over the classical mechanical and thermal methods comes from the strong spatial and temporal localization of the laser-mater interaction which gives very large heating/cooling rates (as large as 1,000 K/ns [1, 7, 8]) and small volumes that are subjected to the thermal induced defects beyond the removed material. Thus, PLA is the adequate method for processing brittle and thermal 'sensitive' materials.

The physics behind PLA lies, at the microscopic level, in photon-electron interaction (inverse Bremsstrahlung effect at fs scale) whereas at later times (ps-ns scale) PLA involves electron-electron and electron-phonon interactions. Thereby, for ns and ps lasers, PLA can be analysed as a simple thermal effect involving heating, melting and vaporization of the target. The fundamental criteria for choosing certain irradiation conditions for high quality ablation of a given material consists mainly of relation between the ablation rate and the thermal and optical penetration depths. Thus, if the ablation rate, defined as the thickness of the ablated layer during a laser pulse, obeys the simple rule [1]

$$\Delta h = \max(l_T, l_\alpha), \tag{1}$$

then all the thermal and optical induced defects are removed during the laser pulse. In Eq. (1) $l_\alpha = 1/\alpha$ and $l_T = \sqrt{D\ t_p}$ are the optical and thermal lengths, $\alpha$, $D$ and $t_p$ represent the absorption coefficient, the thermal diffusivity and the pulse duration, respectively.

When the laser fluence is above the threshold that gives a strong ionization of the ablation vapour (i.e. above the plasma-ignition threshold which is of the order of 10-100 J/cm$^2$ depending on the material and laser wavelength), the optical penetration depth of the plasma should be also accounted for since the plasma acts as a secondary heat source but also as a shield and/or scattering medium for the incoming laser pulse [1, 2, 8].

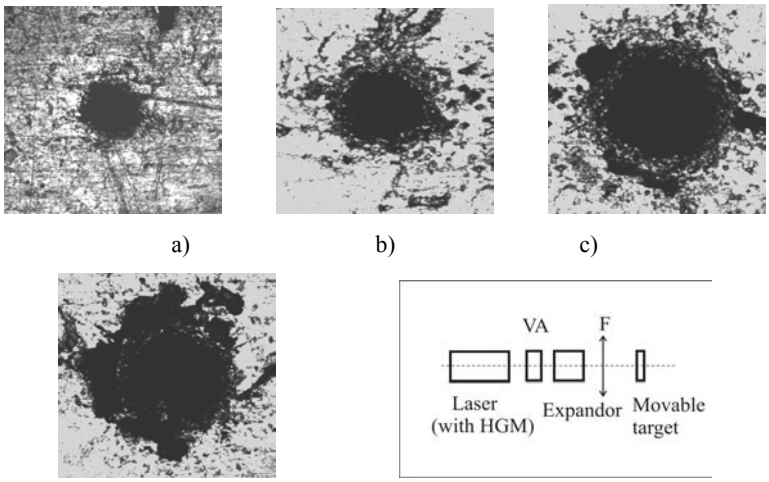


Fig. 1 – a) 200×200 microns confocal microscopy images of craters drilled in aluminium by focusing 20 pulses (532 nm wavelength, 5ns duration) with different energies; b) 0.05; c) 1.5; d) 5 mJ); to a 10 microns diameter spot; the depths of the first three craters are 20, 105 and 210 microns, respectively, whereas their diameters are 60, 120 and 170 microns, respectively; d) a crater corresponding to the out of focus irradiation; e) typical set-up that we used for our PLA experiments.

## 2. EXPERIMENTAL PLA

The ideal laser pulses for PLA are as short as possible so that to reduce the thermal effects induced into the irradiated material, and have a flat intensity profile so that to produce as steep as possible walls for the ablated microstructures. Excimer lasers and solid state lasers such as Ti-sapphire lasers can provide very short pulses (down to tens of fs) and more or less top-flat intensity profile. However, the high-costs for acquisition and long-time running, as well as the technical difficulties in keeping constant parameters for these lasers, limit the number of fs lasers users. Actually, most of the research groups worldwide that work in the field of PLA use ns and ps lasers (such as Nd-YAG and Nd fiber lasers) which are more reliable and cost efficient. The disadvantage of non-uniform Gaussian profile of the laser intensity is usually solved by using diffractive homogenizers whereas the fundamental IR wavelength is reduced by using harmonic generators.

The main irradiation methods for PLA imply either direct scan of the processing beam on the target surface, the projection of the beam through masks, or interference of two secondary beams for ablating periodic structures [1]. We mainly used for our experiments the former configuration, the typical setup being outlined in Fig. 1e. The laser wavelength of the ns Nd-YAG laser is varied by introducing harmonic generation modules (HGM) for the 1064 nm fundamental

beam. The laser fluence is varied by changing the laser energy with a variable attenuator (VA), and the beam diameter is varied by translating the target away from the focal plane of the focusing lens (F).

We analysed the dependence of the ablation rate of metals, semiconductors and dielectrics on different laser parameters: wavelength, fluence, beam diameter and pulse number [9-16]. Thus, the ablation rate decreases with wavelength due to reduced optical absorptivity and high reflectivity of the target surfaces at large wavelengths, as well as to the strong Bremsstrahlung absorption of the large wavelength processing beam into the ablation plasma. Fig. 2a demonstrates that, for a given fluence (e.g. 100 J/cm$^2$ as we chose here), there is a certain decreasing tendency of the ablation rate with wavelength for three different metals (Al, Ti and Cu). This result comes from a set of data (Fig. 2b) regarding the dependence of the ablation rate on fluence at different wavelengths (i.e. 355, 532 and 1,064 nm). The fitting curves describe a logarithmic increase of the ablation rate with fluence [9]:

$$\Delta h = \Delta h_0 \ln(F / F_{th}), \tag{2}$$

where $F_{th}$ is the threshold fluence, which depends on wavelength and material properties.

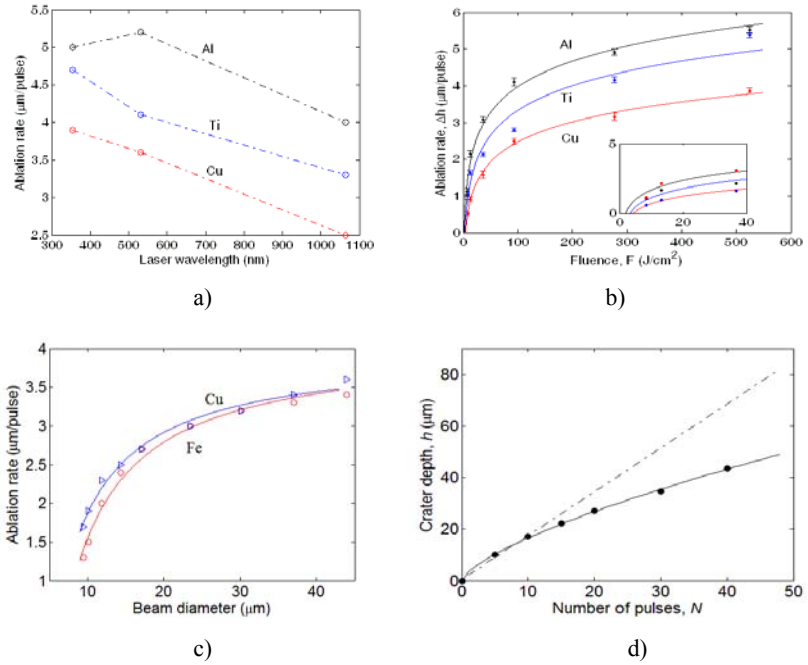


Fig. 2 – a) The dependence of the ablation rate on the laser wavelength and b) on the fluence for Al, Ti and Cu; c) the dependence of the ablation rate of Fe and Cu *vs*. beam diameter at 532 nm and 150 J/cm$^2$; d) the dependence of the crater diameter drilled in $LiNbO_3$ on pulse number.

Increasing the beam diameter by translating the target away from the focal plane, the ablation rate decays linearly with the square-root of the diameter (Fig. 2c). The fitting curves are described by the equation [9]

$$\Delta h = R_{\Delta h}\left(\sqrt{F} - \sqrt{F_{th}}\right), \tag{3}$$

where $R_{\Delta h}$ depends on the thermal diffusivities of the materials.

The ablation rate is also demonstrated to depend on pulse number [1, 8, 10]. Thus, during the first 10-20 pulses, depending on the material properties and wavelength, the ablation rate is almost constant. As the number of laser pulses and the depth of the crater increase, the ablation plasma is trapped inside of the crater, leading to rapid increase of the plasma density and absorption coefficient, and hence to a weak direct coupling of the laser energy to the sample [1, 4, 8]. The non-localised heating of the whole crater-wall produced by the plasma plume ruther than direct heating of the crater tip produced by the laser beam gives the non-linear dependence of the crater-depth and the decay of the ablation rate with pulse number. Fig. 2d) presents the dependece of the depth of the crater drilled in a dielectric target (namely $LiNbO_3$ that is widelly used in optoelectronics) on the pulse number at 10 J/cm$^2$ fluence.

## 3. METHODS FOR PLA ANALYSIS

There are post-processing and real time methods for PLA analysis. The former methods give accurate information about the dimensions and quality of the micro and nano-ablated structures but give no possibility to control the ablation during the process. The above mentioned results concerning PLA were obtained by using post-processing methods such as optical and confocal microscopy. Instead, real-time methods give no so accurate information on the actual quality and geometry of the structures but enable control of PLA during the ablation process, i.e. correction of experimental parameters during laser processing (the pulse number and the axial position of the focus. This is important in order to avoid the effects of random variations of the laser beam parameters (e.g., the peak power of the laser pulse, pulse duration) and of the sample characteristics (e.g., absorbance, reflectance).

### 3.1. OPTO-ACOUSTIC METHODS

Optodynamics allows the study of the both thermal and optical effects induced by the laser radiation, such as the dynamics of the ablation products, ablation plasma, and the generation of shock waves during laser processing of a material [10]. In this study we use a piezoelectric transducer (PZT) connected to a digital oscilloscope to determine the propagation time of the shockwaves through

the target during percussion drilling. The experimental set-up is shown in Fig. 3a. We used a "Brilliant" Q-switched Nd-YAG laser system provided with a second harmonic generator module (SHM). Laser pulses have 4.5 ns with 10 Hz repetition rate, with 360 mJ energy for the fundamental harmonic (1064 nm wavelength). The target was fixed in the lens focus to ensure a maximum irradiation at the target (Fig. 3b). Part of the scattered beam is detected by a photodiode (PD) whose signal triggers the time base of the oscilloscope. The signals from the PZT are digitally acquired on the oscilloscope and then processed and individually analyzed. A typical signal from the PZT during drilling of a copper target is shown in Fig. 3b.

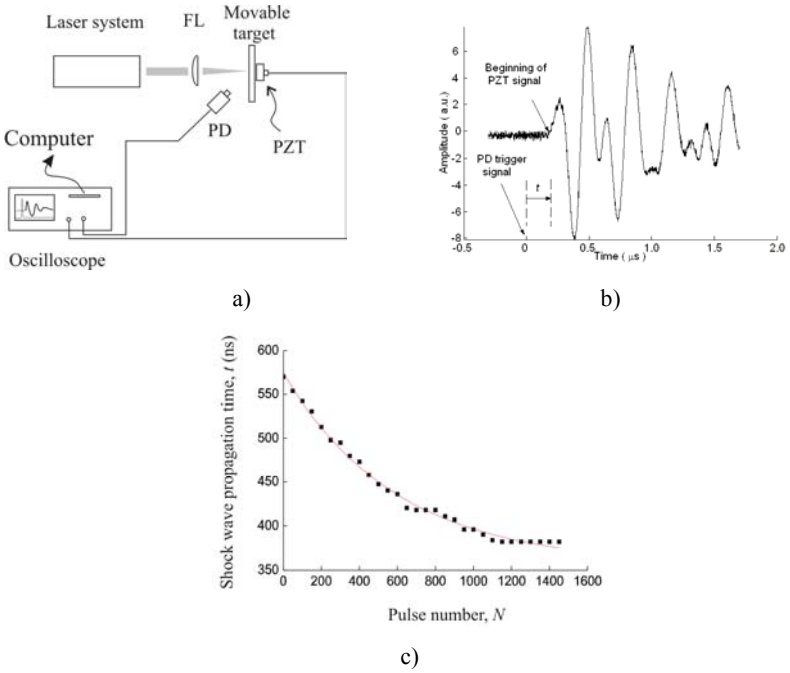


Fig. 3 – a) Real-time determination and control of the laser drilled holes depth. Experimental set-up for determination of the depth $h$ of laser drilled holes; b) determination of propagation time $t$ of the shock waves within the target from a typical signal of the piezoelectric transducer; c) the dependence of the shock wave propagation time on the pulse number for a 2.5 mm thick copper target irradiated with 532 nm laser pulses.

The shock wave propagating through the sample is a superposition of many waves originating from different points in the hole. For simplicity, here we consider that the shock wave originates from a point source at the bottom of the growing hole. With this assumption, the distance from the target surface to the origin of the shock wave is the hole depth $h$, while $l$ is the distance from this origin to the rear target surface where PZT is set (see Fig. 3b). The first amplitude peak of the PZT signal was used to determine the propagation time $t$ of the produced shock wave to the rear surface.

In the early stages of the process, the distance $l$ to the PZT and the propagation time $t$ of the shock waves decreases strongly with the increasing the pulse number, resulting in an approximate exponential decrease of the ablation rate with pulse number. For a certain number of laser pulses (approximately 1000 for aluminium irradiated at 532 nm as indicated in Fig. 3c), the shock-wave propagation time and hole depth cease to have an observable variation due to the less efficient transport of the ablation products out of the crater when the crater depth becomes comparable with the plasma hydrodynamic length. The number of pulses at which this change occurs is strongly dependent on the laser wavelength and on the optical and thermal properties of the material.

## 3.2. SPECTROMETRIC METHODS

The optical methods are precise and powerful tools for analyzing laser induced effects because in many cases they are nondestructive, simple, very fast and sensitive and have high spectral/spatial resolution [16-19]. Plasma formation by intense laser irradiation of solids is the subject of investigations in many fields of applied and fundamental research, from laser-plasma sources to X-ray lasers, from inertial confinement fusion to laboratory astrophysics. The emission spectroscopy has been used in studying plasma generated during incipient stages of PLA. We used the laser spectroscopy of $Er^{3+}$-doped Ti:$LiNbO_3$ plasmas produced by focusing ns Nd-YAG laser pulses on the target surface [16].

The typical experimental set-up used for the spectroscopic characterization of the ablation plasmas is presented in Fig. 4a. The energy of the ns beam is varied so that to obtain a fluence of 0.1 to 10 TW/cm$^2$ at the target surface. The laser is focused at normal incidence on the target and the magnified image of the plasma is scanned with an optical fibre connected to the spectrometer to obtain the spatial distribution of the temperature within the plume. At each position of the monochromator grating corresponding to a certain wavelength, the light intensity was integrated during at least a time equal with the inverse of repetition frequency of the laser shots. Then the emission spectrum is recorded by a computer (Fig. 4b).

The dimensions of the ablated craters were measured using a metallographic microscope having about 1 μm resolution and a confocal microscope Leica Microsystems Heidelberg GmbH. The relative measurement errors are < 5%. The results presented in Fig. 1d) indicates the decay of the ablation rate with pulse number, mainly due to the plasma trapping inside of the craters. The trapping of the plasma inside of the crater is demonstrated by the decay of the lines intensities that are reccorded at a fixed position above the target surface when increasing the number of consecutive pulses impinging the same spot on the target's surface. Part of the visible spectrum of the $Er^{3+}$-doped Ti:$LiNbO_3$ ablation plasma presenting the two main lines of neutral Li atoms at 611 and 671 nm is presented in Fig. 4b.

Increasing fluence leads to the increase of the lines intensity whereas the ratio of the 671 to 611 nm lines intensities keeps almost constant (Fig. 4b). When moving the

observation point into the plume at larger distances (i.e. 1 and 2 mm away) from the target surface, the lines intensities obtained at a given laser irradiance become larger. These observations could suggest that the plasma is either richer in neutral Li atoms or hotter when increasing the laser irradiance and the distance from the target.

In order to decide what the case here is, we analysed in more detail the relative intensities of the 2 lines (Fig.4b) to determine the plasma temperature. We took into account the Boltzmann's distribution of the atoms on the energetic levels of a thin plasma. The electron temperature was estimated by analysing the relative intensities the atomic lines of Li at 610.3 and 670.8 nm presented in Fig. 4b, the atomic data for these lines being given in [20]. Due to a very limited spectral resolution of the measurement system, no line profile analysis was possible. So, no flattening of spectral profile in its center for a homogeneous plasma and no absorption dip for a inhomogeneous plasma could be observed. But, due to the very probable self-absorption of the resonance lines radiation at 670.8 nm in the plasma, the emission coefficient corresponding to these lines is under-estimated. This fact leads to an estimated value of the electron temperature greater than the real value.

The results presented in Fig. 4c indicate that the plasma temperature is ~14,000 K, being non-dependent on the laser irradiance or the position within the plume. Thereby, the difference in the lines intensities observed in Fig. 4b comes only from the richness in neutral Li atoms that are obtained at high laser irradiances. In fact, the increase of laser irradiance leads to larger volumes of ablated material rather than by heating the plume.

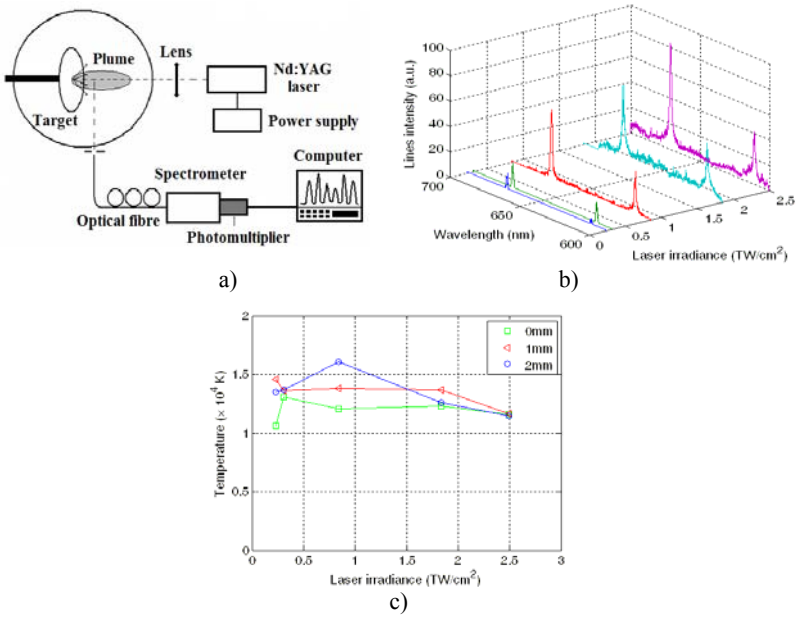


Fig. 4 – a) The scheme of the experimental setup for plasma spectroscopy; b) the visible spectrum of the $Er^{3+}$:Ti:$LiNbO_3$ plasmas at the target surface for different attenuator positions; c) the plasma temperature as a function of laser irradiance for different positions within the plasma plume.

## 4. THEORETICAL MODELING OF PLA

PLA in nanoseconds and picoseconds regimes within the theoretical photo-thermal model is considered as a superposition of heating, melting, vaporization and melt ejection under the action of the plasma recoil pressure. The comparison of the theoretical results on the ablation rate with experiments indicates two main mechanisms that contribute to the decrease of the ablation efficiency in multi-pulse regime. First, during first stages of PLA, the absorbing laser-plasma expanding above the irradiated target attenuates the laser beam that reaches the target, leading to a marked decrease of the ablation efficiency. The second mechanism which determines the decrease of the ablation efficiency consists in the reduction of the incident laser irradiance with the lateral area of the ablated structure, and in the melt ejection velocity with the depth of the hole.

We use Cranck-Nicholson finite-difference method in an iterative algorithm for solving heat equation corresponding to the photo-thermal model. In a coordinate system that is fixed to the irradiated surface that recedes due to ablation, the one-dimensional heat equation describing the propagation of the heat flow and of the melting/solidification front into the irradiated sample can be written as [1, 2, 4, 8]:

$$\begin{aligned} &\rho\left[c_p + \Delta H_m \delta(T - T_m)\right]\left(\frac{\partial T}{\partial t} - v_a \frac{\partial T}{\partial z}\right) - k\frac{\partial^2 T}{\partial z^2} = \\ &= (1-R)\alpha I \exp(-\alpha z - \int \alpha_{pl} v_{pl} \mathrm{d}t), \end{aligned} \tag{4}$$

where $\rho$, $c_p$, $\Delta H_m$ and $k$ denote the density, the specific heat, the melting enthalpy at normal melting point, and the thermal conductivity of the metallic material, respectively, taken as constant, temperature-independent parameters. $v_a$ is the ablation velocity, $R$ and $\alpha$ represent the reflectivity and absorption coefficient of the target, and $I$ describes the time variation of the laser pulse intensity. The absorbent plasma that expands away from the target with a hydrodynamic velocity $v_{pl}$ has the optical absorption coefficient $\alpha_{pl}$. The hydrodynamic velocity of the plasma-plume can be approximated by [1]:

$$v_{pl} = \sqrt{0.67\gamma k_B T_s / M}\,, \tag{5}$$

where $\gamma$, $M$, $T_s$ and $k_B$ are the adiabatic coefficient, the atomic mass of the target, the target surface temperature, and the Boltzmann constant, respectively. The ablation velocity due to evaporation is given by the Hertz-Knudsen equation [1]

$$v_a = 0.32\sqrt{\frac{M}{k_B T_s}}\frac{p_s}{\rho}, \tag{6}$$

where $p_s$ is the saturated vapour pressure above the surface, being given by the Clausius-Clapeyron equation [1, 2, 4, 8]. The correction coefficients 0.67 in Eq. (5) and 0.32 in Eq. (6) account for the influence of the Knudsen layer on the plasma parameters [1]. That is, the correction coefficients account for the backward flux of particles, for the partial transformation of the thermal energy into hydrodynamic kinetic energy of the plume, and respectively for the over-saturation and condensation of the vapour. The melt ejection is also accounted for in calculating the ablation velocity by using the hydrodynamic Bernoulli law for the melted layer around the crater under the piston-like action of the recoil pressure of the ablated plasma [1,2]. Thereby, the ablation rate $\Delta h$ is obtained by time integrating the ablation velocity over the repetition period of the laser pulses.

The difficulties in solving the heat equation comes from the dependence of the ablation velocity, the plasma absorption coefficient, and the plasma-plume velocity that appear as parameters in the heat equation (4) on the temperature of the target surface. In order to overcome this difficulty, we used a multi-step method for integrating the heat equation. The multi-step method is described in what follows. At small pulse frequencies (i.e. up to 1 kHz), the irradiated surface is cooled to the ambient temperature $T_{amb}$ before each consecutive laser pulse [1,8]. Thus, the initial condition of the heat equation is $T(z, t=0) = T_{amb}$.

The boundary conditions of the problem are as follows: the Dirichlet-type boundary condition at rear surface $T(z=h, t) = T_{amb}$ indicates the small thermal penetration depth relative to the target thickness, whereas the Newmann-type boundary condition at the irradiated surface ($z = 0$) gives the energy balance here:

$$k \left.\frac{\partial T}{\partial z}\right|_{z=0} = \rho v_a \, \Delta H_v \,. \tag{7}$$

The temperature distribution within the target obtained at the end of first integration step is used as initial condition for the next integration step. The time variation of the surface temperature during the first integration step gives the ablation velocity, the plasma plume velocity, and the plasma absorption coefficient which are used as parameters in the heat equation (4) and into the boundary condition (7) for the next integration step. The heat equation is then integrated for the remaining time steps of the laser pulse following the same procedure as for the first step.

Typical results on ablation rate obtained when using metallic targets within this model are presented in Fig. 5. The computed and experimental values of the sample thickness as a function of the laser pulses number (doted curve in Fig. 5 b)), are fitted with the same type of exponential function

$$h = h_f + (h_i - h_f)\exp(-2N / N_{th}) \quad \text{[mm]} \tag{8}$$

where $N_{th}$ is the threshold value for the number of consecutive laser pulses corresponding to a zero ablation rate, and $h_i$ and $h_f$ are the initial and the final thickness of the sample, respectively. Then, the ablation rate is derived as the ratio of crater depth and pulse number.

There is reasonable agreement between the values of the theoretical and experimental results as indicated in Fig. 5b. Fig. 5c indicate that the ablation rate of Al is almost constant during the first 20 pulses and decreases stronger and stronger as the pulse number increases.

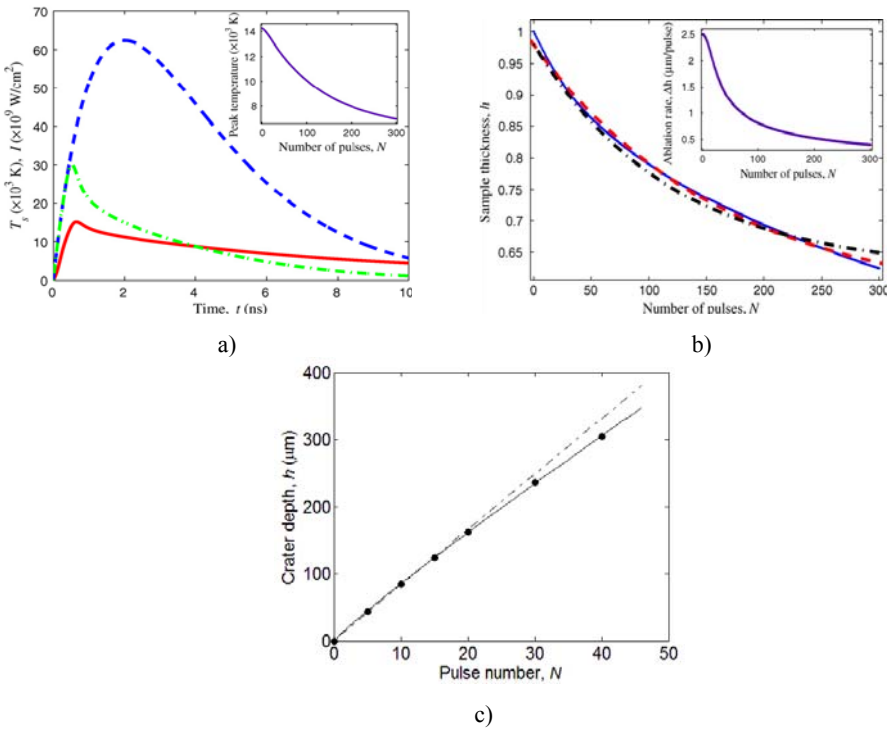


Fig. 5 – a) The time-dependence of the target-surface temperature (solid line), laser intensity (dashed line) and effective irradiance at the target accounting for the plasma shielding (dash-dotted line). The dependence of the peak temperature on pulse number is given in the inset; b) the thickness of Al target (in mm) *vs*. pulse number obtained by computations (solid line) and the experimental data [8] (dash dotted line). The dependence of the ablation rate on the number of laser pulses is given in the inset; c) experimental dependence of the crater depth in Al on pulse number at 10 J/cm$^2$.

## 5. CONCLUSIONS

We analysed the dependence of the ablation rate of metals, semiconductors and dielectrics on different laser parameters: wavelength, fluence, beam diameter

and pulse number. The ablation rate decreases with wavelength due to reduced optical absorptivity and high reflectivity of the target surfaces at large wavelengths, as well as to the strong Bremsstrahlung absorption of the large wavelength processing beam into the ablation plasma. Increasing the beam diameter by translating the target away from the focal plane, the ablation rate decays linearly with the square-root of the beam diameter. The ablation rate is also demonstrated to depend on pulse number. Thus, during the first 10-20 pulses, depending on the material properties and wavelength, the ablation rate is almost constant. As the number of laser pulses and the depth of the crater increase, the ablation plasma is trapped inside of the crater, leading to rapid increase of the plasma density and absorption coefficient, and hence to a weak direct coupling of the laser energy to the sample

Most of the experimental results regarding PLA were obtained by using post-processing methods such as optical and confocal microscopy. We presented also an opto-acoustic method that allows the study in real time of both thermal and optical effects induced by the laser radiation, such as the dynamics of the material removed and the generation of shock waves during laser processing of a material. Additionally, we studied by emission spectroscopy the the visible spectrum of the $Er^{3+}$-doped Ti:$LiNbO_3$ ablation plasma. The results indicate that the plasma temperature is ~14,000 K, being non-dependent on the laser irradiance or the position within the plume. The observed difference in the lines intensities are determined only by the richness in neutral Li atoms that are obtained at high laser irradiances. The increase of the laser irradiance leads to larger volumes of ablated material rather than by heating the plume.

The experimental results on PLA in nanosecond and picosecond regime can be understood within the photo-thermal model which considered PLA as a superposition of heating, melting, vaporization and melt ejection under the action of the plasma recoil pressure. The comparison of the theoretical results on the ablation rate with experiments indicates two main mechanisms that contribute to the decrease of the ablation efficiency in multi-pulse regime. First, during first stages of PLA, the absorbing laser-plasma expanding above the irradiated target attenuates the laser beam that reaches the target, leading to a marked decrease of the ablation efficiency. The second mechanism which determines the decrease of the ablation efficiency consists in the reduction of the incident laser irradiance with the lateral area of the ablated structure, and in the melt ejection velocity with the depth of the hole.

## REFERENCES

1. D. Bauerle, *Laser processing and chemistry*, Springer-Verlag, 2000.
2. M. v. Allemen, A. Bllatter, *Laser-Beam Interaction with Materials*, Springer-Verlag, 1995.
3. J. F. Ready, *Effects of High-Power Laser Radiation*, Academic Press, New York, 1971.

4. N.M. Bulgakova and A.V. Bulgakov, Appl. Phys., A **73**, 199 (2001).
5. M. Stafe, I. Vladoiu, C. Negutu and I.M. Popescu, ICALEO Conf. Proc., P130 (2008).
6. *** ICALEO Conference Proceedings, 2008.
7. B.N. Chichkov *et al.*, Appl. Phys., A **63**, 109 (1996).
8. M. Stafe, C. Negutu, I.M. Popescu, Appl. Surf. Sci., **253**, 6353 (2007).
9. M. Stafe *et al.*, Proceedings of SPIE ,**7426**, art. no. 742614 (2009).
10. M. Stafe, C. Negutu, I.M. Popescu, Shock Waves, **14**, 123, (2005).
11. M. Stafe, I. Vladoiu, I.M. Popescu, Cent. Eur. J. Phys., **6**, 327 (2008).
12. M. Stafe, I. Vladoiu, C. Negutu, I.M.Popescu, Sci. Bulletin of Univ. "Politehnica" of Bucharest, Series A: Applied Mathematics and Physics, **71**, 73 (2009).
13. I. Vladoiu, M. Stafe, C. Neguțu, I.M. Popescu, Sci. Bulletin of Univ. "Politehnica" of Bucharest, Series A: Applied Mathematics and Physics, **70**, 119 (2008).
14. M. Stafe, I. Vladoiu, C. Negutu, I.M. Popescu, Rom. Rep. Phys., **60**, 789 (2008).
15. I. Vladoiu, M. Stafe, C. Negutu, I.M. Popescu, Eur. Phys. J.-Appl. Phys., **47**, 30702 (2009).
16. C. Negutu, M. Stafe, S. S. Ciobanu, I. Vladoiu, N. N. Puscas, Sci. Bulletin of Univ. "Politehnica" of Bucharest, Series A: Applied Mathematics and Physics, **70**, 85 (2008).
17. S. Amoruso *et al.*, J. Phys. B: At. Mol. Opt. Phys., **32**, 131 (1999).
18. I. Pauleau, *Laser Beam-Solid Interactions: Fundamental Aspects*, Elsevier, 2005.
19. J. Lamela et al, Appl. Surf. Sci. **255**, 3918 (2009).
20. NIST, Joseph Reader et al., *Wavelengths and Transition Probabilities for Atoms and Atomic Ions*. Part 1. *Wavelengths*, Part 2. *Transition Probabilities*, NSRDS-NBS 68 (1980).